VTT Technical Research Centre of Finland

Online nonlinear ultrasound imaging of crack closure during thermal fatigue loading

Koskinen, Tuomas; Kuutti, Juha; Virkkunen, Iikka; Rinta-aho, Jari

Published in:
NDT & E International

DOI:
10.1016/j.ndteint.2021.102510

Published: 01/10/2021

Document Version
Publisher's final version

NDT&E International 123 (2021) 102510

Contents lists available at ScienceDirect

NDT and E International

journal homepage: www.elsevier.com/locate/ndteint

Online nonlinear ultrasound imaging of crack closure during thermal fatigue loading

Tuomas Koskinen [a,*], Juha Kuutti [a], Iikka Virkkunen [b], Jari Rinta-aho [a]

[a] VTT Technical Research Centre of Finland, Finland
[b] Aalto University, Finland

ARTICLE INFO

Keywords:
Thermal fatigue
Crack closure
Ultrasound
Fundamental wave amplitude difference
Nonlinear ultrasound

ABSTRACT

A thermal fatigue surface crack (6 mm deep × 23 mm wide) in a thick austenitic stainless steel plate is opened and closed with thermal heating and cooling cycles. This closing and opening of the crack is recorded with using fundamental wave amplitude difference (FAD) technique with 5 MHz 64 element phased array probe. In addition, the contact pressure and crack opening state at different time intervals were estimated using finite element (FE) simulation. In combination with the nonlinear output from the FAD and FE simulation gave insight at which level the contact pressure or the distance between crack faces prevents the contact acoustic nonlinearity (CAN) from happening. Predictably, no clear nonlinear response was recorded at crack face locations experiencing high contact pressure and on the locations where the crack could be considered fully open, as predicted by the FE simulation. Therefore, the FAD technique can be utilized within the constraints quantified in the paper.

1. Introduction

Nuclear power plants (NPPs) have been built for long term use and as this long term use is extended beyond the original design life, reliable non-destructive inspections (NDI) have a huge impact on the safe operation of the NPPs. Austenic stainless steel materials are widely used in critical components such as primary circuit piping. These components are usually inspected with ultrasonic testing to detect possible cracking caused by the thermo-mechanical loads and corrosive environment. When such cracks are found, proper sizing of the indications is critical for accurate assessment of the flaw acceptability.

The ultrasonic inspections are typically performed while the plant is offline and cooled down to ambient conditions. In traditional ultrasonic inspection, the linear response from an open crack is mainly based on the difference between the acoustic impedance of two different mediums. As there is air inside the crack, the ultrasound is reflected back due to large acoustic impedance difference between air and metal. As the ultrasound is reflected back to the probe from the crack interface, the received signal has the same frequency as transmitted signal. Traditional linear ultrasonics focus only on this central frequency [1–3].

Residual stresses may cause a crack that is open during normal operation to close as the plant is being shut down [4,5]. In the presence of residual stresses, other structural constraints or even an oxide film Takumi et al. [6], the crack faces may remain in contact with each other making the crack particularly difficult to find with ultrasound. The ultrasonic wave is fully or partially transmitted over the closed defect, as there is no acoustic impedance difference to reflect the ultrasound back. Thus, the linear ultrasound inspection would not detect this crack, or it could underestimate the crack size if the crack tip remains closed or classify the crack as subsurface if the mouth is closed [1–3]. Partially or fully closed cracks are mechanically no less critical as there is no significant cohesion between the crack faces.

If the crack faces are completely or partially closed, linear ultrasound passes trough these cracks without significant response. Nonlinear ultrasonics are utilized to detect this kind of cracks. Nonlinear ultrasonic response is traditionally generated from the edges of the crack with approximately double the frequency and half the frequency of the original wave. Usually, this scattering from the crack edges is subtle and the effect is enhanced with special transducers capable of high voltage inputs. As the voltage increases, the scattering causes the effect of super harmonics to be generated from the open parts of the crack as well [7]. As the super harmonics overlap the linear response, subharmonics have been utilized to distinguish the open and closed parts of the crack in more detail [8–11]. The downside of utilizing subharmonic ultrasonic

* Corresponding author.
E-mail addresses: tuomas.koskinen@vtt.fi (T. Koskinen), juha.kuutti@vtt.fi (J. Kuutti), iikka.virkkunen@aalto.fi (I. Virkkunen), jari.rinta-aho@vtt.fi (J. Rinta-aho).

https://doi.org/10.1016/j.ndteint.2021.102510
Received 9 June 2021; Accepted 20 July 2021
Available online 24 July 2021

waves is that they require special equipment to produce and detect such as the subharmonic phased array for crack evaluation approach (SPACE) Ohara et al. [7]. In solid materials, this nonlinear effect from the closed crack is caused by contact acoustic nonlinearity (CAN). The nonlinear effect is generated when the faces of the crack interact with each other. As the crack faces are close enough, they start *"clapping"* due to resonance effect [12–14]. Thermal fatigue crack are typically rough and there are some parts and sections which are closed enough to generate this effect, especially toward the crack tip.

Recently, studies by Haupert et al. [15,16] have been published where nonlinear ultrasound was applied to characterize a surface flaw manufactured using controlled thermal fatigue loading. The same principle has been used for closed fatigue crack by Ikeuchi et al. [17] and a mechanical fatigue crack in a CT specimen by Ohara et al. [18]. The novelty in the research by Ikeuchi et al. [17]; Haupert et al. [15,16]; Ohara et al. [18] was the use of conventional phased array probes and normal inspection equipment. This is achieved by the fundamental wave amplitude difference (FAD) technique [17]. As nonlinear responses have required special transducers with high voltage to clearly detect these elusive frequencies, FAD can be utilized with traditional phased array probes with constant input voltage by using three subsets of element sequences during data acquisition; full aperture, odd elements and even elements. The principle behind FAD relies on the assumption that the fundamental amplitude experiences a fundamental loss as the crack face interaction generates subharmonics $f/2$ and superharmonics $2f$. The full aperture produces the highest amplitude response, while the odd and even elements achieve approximately half of the full aperture's amplitude and therefore the nonlinear response from the odd and even elements is approximately a quarter of the full aperture's nonlinear response. Once the response from the odd and even elements is summed together and extracted from the full aperture's response, the outcome shows indirectly the nonlinear response from the crack. The principle behind FAD is well explained by Ikeuchi et al. [17]; Ohara et al. [18]. Moreover, FAD method is similar to scaling substraction method by Scalerandi et al. [23], where the nonlinear response is calculated by comparing reference signal and larger amplitude signal. FAD seems to be highly feasible approach to detect and size closed or partially closed cracks, however the limitations and constraints of the approach need to be known in more detail before this technique can be reliably utilized in NPP non-destructive inspections.

In this paper, we present an instrumented thermal fatigue experiment where a surface crack is periodically opened and closed with different loading rates and heat inputs. The loading will expose the crack to different contact pressures and crack openings, which are numerically quantified with finite element (FE) simulations. We monitor this closing and opening during the experiment with the FAD approach and compare the measured responses with the contact pressure from the FE simulation. In addition, the crack mouth opening behavior is quantified from visual observations. This provides quantified information when the FAD approach is needed to characterized the crack accurately.

2. Methods

The thermal fatigue experiment was performed on a similar surface crack sample to that used by Haupert et al. [15]. The sample was produced at Trueflaw Ltd. using identical manufacturing parameters. This sample was scanned after manufacturing to characterize the crack using linear and nonlinear ultrasound techniques. Then the sample was re-subjected to cyclic thermal loading tailored to open and close the crack in a controlled fashion during which the ultrasound scanning was being performed. The applied thermal cycle was designed to produce notable crack opening and closure phases and an intermediate phase where the crack faces are partially open. This allows the quantification of the detection capability of the nonlinear ultrasound technique with respect to the strength of crack closure. Additionally, accompanying finite element analyses were performed to validate the ultrasound imaging findings and provide additional information of the crack behavior during the load cycle.

2.1. Manufacturing of thermal fatigue crack and thermal loading

The sample was manufactured using controlled thermal fatigue loading with Trueflaw Ltd. proprietary process [19]. Located on the surface of a 60 mm thick austenitic stainless steel plate, the validated crack size was 23 mm × 6 mm (length × depth). After production, the crack was re-attached to the loading rig to apply the subsequent thermal loading cycles. The loading cycles were similar to those used during the initial crack production, but were varied to provide varying crack closure response for the present study. The crack opening was monitored from the surface during the loading by a video camera, to obtain an estimate of the crack closure over time. The crack was partially obscured by the loading coil, and thus the opening measurements should be considered indicative only.

Two thermal loading cycles were selected for further investigation: 10 s cycle and 2.5 s cycle. The 10 s cycle consisted 10 s of heating to obtain a maximum surface temperature of 310 °C and 10 s of water cooling. The 2.5 s cycle consisted 2.5 s of heating to obtain a maximum surface temperature of 330 °C and 2.5 s of water cooling.

2.2. Nonlinear ultrasound technique

The instrumentation of the experiment was similar to the studies made by Haupert et al. [15,16]; Ohara et al. [18] with the exception that the phased array probe was glued stationary on the intact surface of the sample, situated on the opposite side to the thermal fatigue crack. The scanning setup is illustrated in Fig. 1. The probe used was Imasonic 64 element phased array probe with the central frequency of 5 MHz. The data was continuously recorded during the thermal fatigue cycle with Zetec Dynaray Lite with acquisition rate of 26.6 Hz, 16 bit depth and 100 MHz digitizing frequency. The recording was divided into three channels; full aperture, even elements and odd elements. The signal was band pass filtered between 2 MHz and 10 MHz frequency to reduce electrical noise caused from the thermal fatigue cycle. The focal point was set with dynamic depth focusing from 16 mm to 57 mm. The overall thickness of the specimen was 60 mm. The angle of the sound beam was moved from −3.6° to 3.6° with a 0.3° step to scan the area around the crack as well. Only the 0° scan was used for nonlinear, subharmonic and superharmonic responses.

Ultrasonic data was recorded over multiple identical thermal and cooling cycles. The second and third consecutive cycles were chosen for closer study. The data was processed the same way as in Haupert et al. [15,16]; Ohara et al. [18]. Equation 1 demonstrates the processing principle. The odd and even channels are summed together and extracted from the full aperture channel to achieve the nonlinear response. In order to achieve better image quality and noise reduction, the nonlinear response was band pass filtered around the central frequency with a Butterworth band pass filter. In addition, $f/2$ subharmonic and $1.5f$ and $2f$ super harmonic responses were filtered with band pass filters from the full array signal data. The software filtering was implemented in Python using the SciPy library Virtanen et al. [20].

$$nonlinearresponse = Fullaperture - (Oddelements + Evenelements) \quad (1)$$

2.3. FE simulation

The response of the crack to the transient thermal load was studied numerically using finite element analysis. A finite element model containing the surface crack was constructed using Abaqus FE software [21]. The model was excited by the prescribed thermal cycle applied to the surface loading area. The thermal stress analysis was performed sequentially coupled such that the heat transfer analysis was performed first and the resulting temperatures for all nodes of the model were used

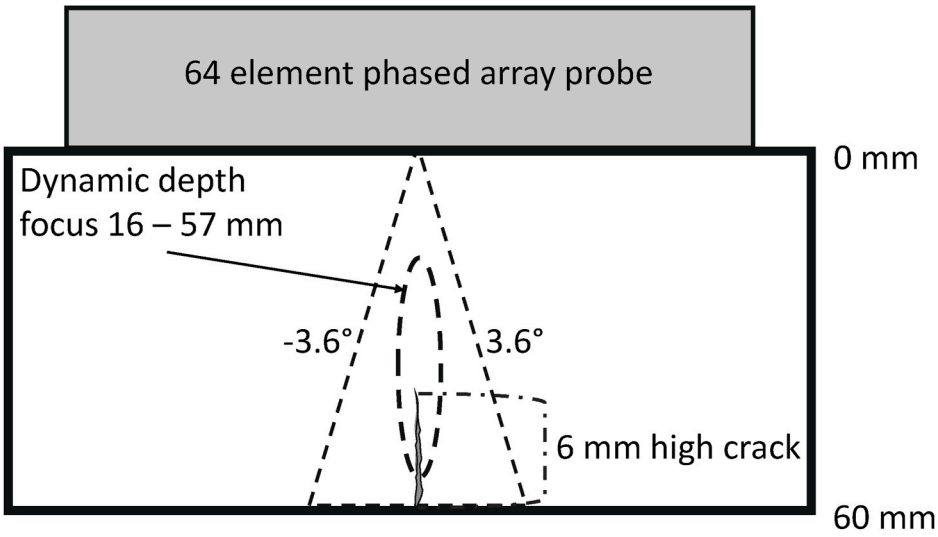

Fig. 1. The setup for recording. A 64 element phased array probe was glued on the opposite surface of the sample to the thermal fatigue crack (23 mm × 6 mm). Electronic scanning was used to scan the crack region from −3.6° to 3.6° angle in 0.3° steps. Dynamic depth focusing was utilized from 16 to 57 mm. Full aperture of the probe was used.

as predefined conditions in the stress analysis. The purpose of the finite element simulations was to predict how the crack faces will open and close during the thermal cycle and provide quantified information of the crack opening displacement and contact stress to help the interpretation of the nonlinear ultrasound characterization of different regions of the crack.

The 3-D FE model of the test specimen used in the simulations is shown in Fig. 2. Different meshes were used in the heat transfer and thermal stress analyses and the transfer of the temperatures from the heat transfer model into the structural model was done via spatial interpolation. The heat transfer and thermal stress meshes consisted of 184976 and 162752 linear 3-D heat transfer and reduced integration structural elements, respectively. The average element edge length in the crack region was 0.25 mm. Symmetry planes were utilized such that only a quarter of the crack was modelled. Crack face contact was modelled using a rigid plate placed on the symmetry plane. The default "hard" contact properties in Abaqus were used with no crack plane friction. The model was otherwise constrained only against rigid body motion.

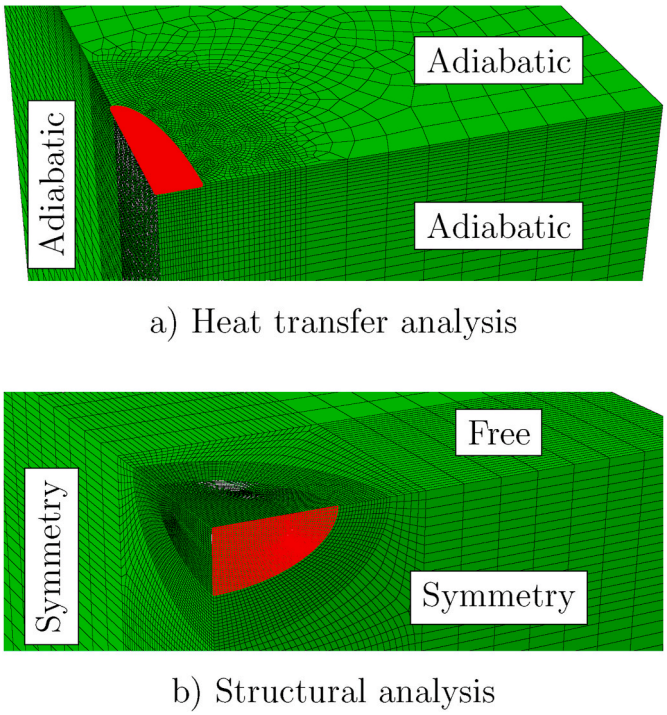

Fig. 2. Close-ups of the finite element meshes used in the heat transfer and thermal stress simulations. The top surface in the figures is the free cracked surface of the specimen and the red areas denote the heating area and crack faces, respectively. (For interpretation of the references to colour in this figure legend, the reader is referred to the Web version of this article.)

The thermal load was applied as a time-dependent temperature boundary condition acting on a small elliptical area surrounding the crack mouth. Other surfaces of the model were assumed to be perfectly adiabatic. An example of the specified temperature cycle shown in Fig. 3. The temperature cycle represents both the induction heating and water spray cooling phases of the experiment. The heating phase of the cycle increases the surface temperature uniformly and linearly up to the maximum temperature, after which the cold water spray decreases the temperature quickly to the ambient temperature. The water spray continues over the cooling phase of the cycle keeping the whole thermally cycled area cool. Both loading cycles, 10 s and 2.5 s, were considered in the simulations. Both cycles were equally divided between the heating phase with linearly increasing temperature and the cooling phase, where the surface temperature was kept low.

The simulations assumed linear heat transfer behavior and perfect elasticity. The material properties used in the simulations were obtained from the ASME B&PVC Section II Part D [22]. The code provides the temperature-dependent properties for stainless steels shown in Fig. 4. In addition to the data shown in the figure, material density of 8030 kg/m^3

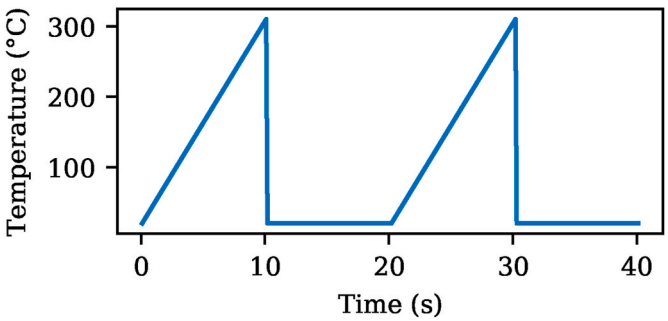

Fig. 3. Two counts of the 10 s thermal cycle applied to the heating area.

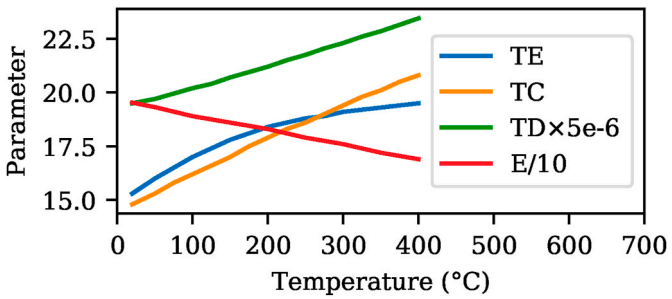

Fig. 4. Material properties used in the simulations. TE, TC, TD and E denote the thermal expansion coefficient (W/m/K), thermal conductivity (W/m), thermal diffusivity (m^2/s) and elastic modulus (GPa). Note that TD and E are scaled by a factor of 5e-6 and 1/10, respectively, in the figure.

and Poisson ratio of 0.31 were used.

3. Results

The results have been divided into two sections. The results from the FE simulation can be found in Section 3.1 and the results from the ultrasonic measurements are in Section 3.2. The indicative crack opening measured from the video recording can be seen in Fig. 5.

Fig. 5 shows that the cooling phase opens the crack faster than the heating phase starts to close it. In the 10 s cycle case, the crack surface opens quickly. Between 2 s and 5 s into the cooling phase, the crack surface closes slightly. After 5 s, the crack surface starts to open again. As the heating starts at 20 s, crack starts to close until 3 s into the heating cycle. In the 2.5 s cycle case, the crack opening is more subtle in the cooling phase. Once the heating starts, the crack starts to close after 1 s into the heating phase. When compared to the longer thermal loading cycle, the shorter cycle opens the crack clearly less because of the shorter time available for the heat flux to propagate into the material.

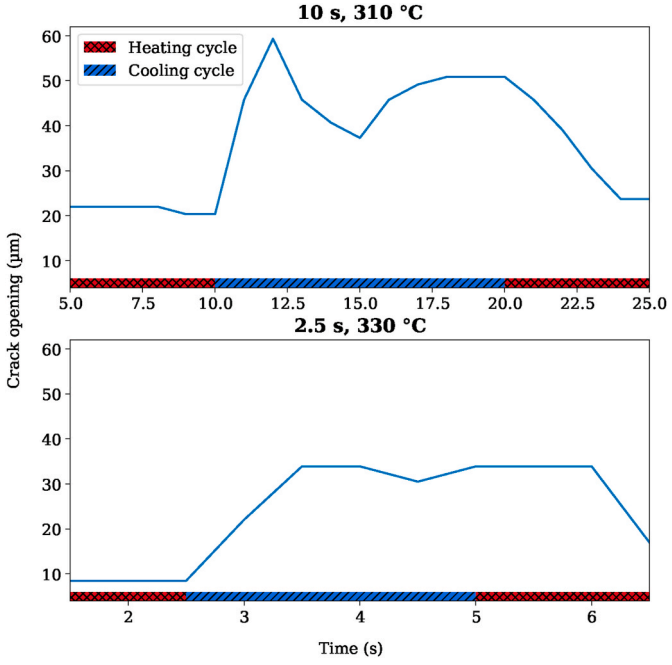

Fig. 5. The crack openings measured from the video feed (above: 10 s thermal load cycle, below: 2.5 s cycle). The cooling cycle is shown as slash hashed blue line underneath the image and the heating cycle as cross hashed red line. (For interpretation of the references to colour in this figure legend, the reader is referred to the Web version of this article.)

3.1. Finite element modelling results

Extracted from the simulation results, Fig. 6a–b and 7 a-b show the simulated temperature and crack opening displacement cycles taken from specified points in the depth direction along the crack center line. Only a single load cycle is shown in the figure with the time axis adjusted such that the maximum crack opening displacement is located near the center of the time axis. Fig. 6c–d and Fig. 7c–d show the magnitude of the crack face contact stress and the state of the crack face opening as a function of the loading cycle time. The results in subfigures a-c were directly obtained from the finite element simulation results. The crack opening state in subfigures d is categorized from the crack face contact stresses such that all node points with zero contact stress are classified to be open, while the nodes where the contact stress exceeds 100 MPa are classified to be closed. The partial contact regions are the nodes with the contact stress between 0 MPa and 100 MPa.

The results obtained from the simulation with the 10 s load cycle are shown in 6 and the results obtained from the simulation with the 2.5 s load cycle are shown in 7.

3.1.1. FE results discussion

The heat applied to the surface propagates into the material slowly. The temperature oscillation at the crack tip depth is smaller than at the surface. The longer 10 s load cycle is able to open the crack tip momentarily before the heating phase of the cycle induces crack closure. The crack mouth and tip are the first to close as heating phase begins. The middle areas of the crack remain momentarily open after the surface temperature has started to increase. The crack faces remain in soft contact for the first seconds of the heating phase, but the whole crack is in strong compression at the end of the heating phase.

The simulation with the shorter 2.5 s load cycle indicates that the thermal inertia prevents the crack tip from experiencing any significant tensile stresses and the tip remains at least in partial contact throughout the loading cycle. The crack opens up to only a half of its depth at maximum before the next heating phase closes the crack quickly.

3.2. NDE characterization

The nonlinear component was calculated as introduced in Section 2.2. The 0° nonlinear response directly above the crack was chosen to be plotted over the thermal fatigue cycle. The nonlinear responses caused by the thermal cycles introduced in Section 2.1 are shown in Fig. 8 for the 10 s, 310 °C cycle and in Fig. 9 for the 2.5 s, 330 °C cycle, respectively. In the figures, the intensity of the bottom surface (crack surface) echo is plotted at the top, the linear response in the middle and the nonlinear response in the bottom image. The depth of the ultrasonic response is plotted at the y-axis (mm) with 0 mm representing the cracked surface of the sample and the time (s) elapsed within the thermal cycle at the x-axis. Furthermore, a logarithmic transformation was taken and the signal was max-pooled for better visualisation of the changes during the cycle.

Fig. 8 shows how the strongest back wall echo is recorded at the end of the heating phase. The strongest nonlinear responses are achieved at 0.7 s ⋯ 1.9 s from the beginning of each cycle. On both counts, the crack opens to 6 mm in depth. 6 s into the cooling phase, a nonlinear response can be observed around the crack tip of 5 mm ⋯ 6 mm. The crack tip is visible during the heating phase, from 4.5 s to 9 s. The same observations apply for the linear response, although the nonlinear response is more visible.

In Fig. 8, nonlinear indications can be observed when the cooling or the heating phases initiate in the 10 s thermal cycle. The bottom echo behaves as expected and the highest response occurs at the end of the heating phase. At the end of the heating phase, no nonlinear or linear responses can be observed beside the clear bottom echo. During the cooling phase, the bottom echo weakens as the ultrasound diffracts from other locations on the crack faces. Right at the beginning of the cooling

phase, the crack opens from the mouth, similar to the prediction made by the FE simulation in Fig. 6. However, the measured opening is faster than in the FE simulation. In the middle of the cooling phase at 6 s, a nonlinear response from the crack tip can be seen momentarily. This slight indication might be related to the closing effect observed in Fig. 5 at the same time interval. Once the cooling phase ends and the heating starts at 20 s and 40 s, no nonlinear response was recorded until from 2 mm at 1 s into the cycle to 6 mm, 2s into the cycle as the crack starts to close. After 2 s into the heating phase, the nonlinear response fades away. Around 4.5 s into the heating phase, the crack tip can be detected until 9 s. After the 9 s of heating, no nonlinear response can be recorded before the cooling phase starts.

As the nonlinear response is based on the fundamental amplitude difference, the changes can be observed on the linear response as well. However, the responses are much difficult to observe than for the nonlinear response.

Fig. 9 shows how the maximum bottom echo is achieved at 1.3 s into the heating phase. A nonlinear indication appears at the beginning of the cooling phase and remains visible for about 1 s in duration and 5.5 mm in height. No nonlinear response can be observed within the heating phase.

In Fig. 9, the nonlinear indication caused by the 2.5 s cycle is similar

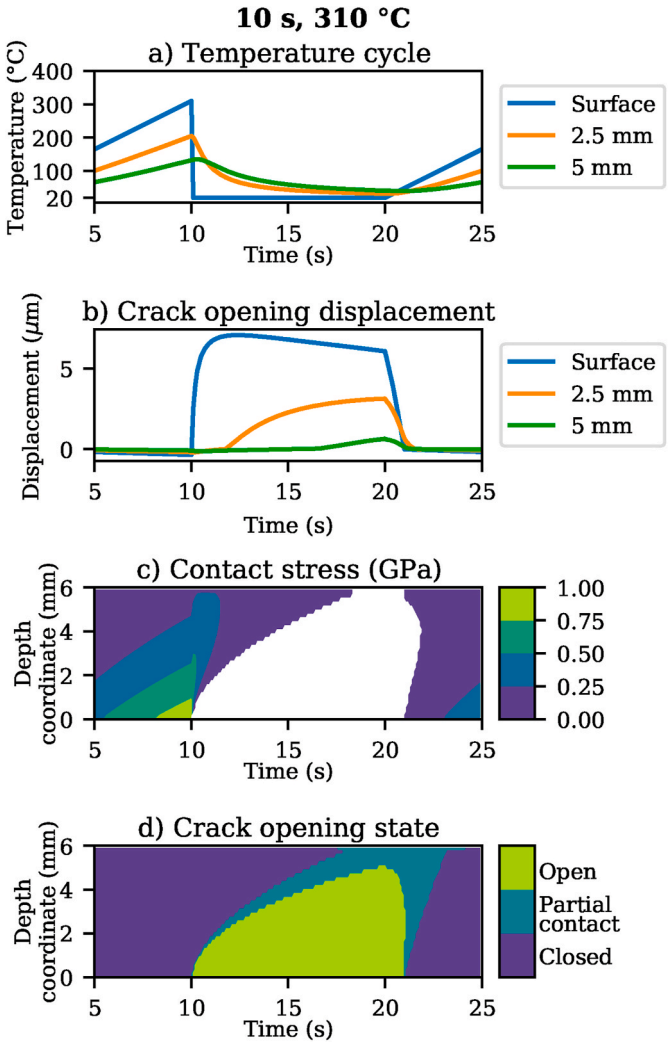

Fig. 6. The temperature cycles (a), crack opening displacements (b) and crack face contact stress (c) and crack opening state (d) over the 10 s thermal load cycle obtained from the finite element simulation. The results are taken from the crack center line from different depths. The crack tip is located at a depth of 6 mm in the figure.

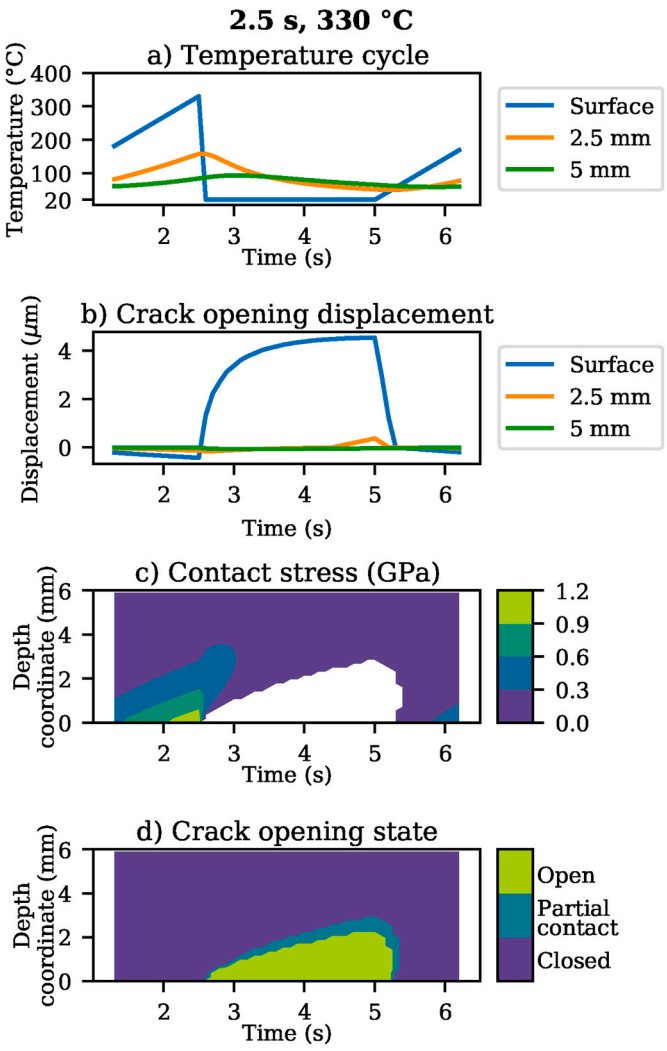

Fig. 7. The temperature cycles (a), crack opening displacements (b) and crack face contact stress (c) and crack opening state (d) over the 2.5 s thermal load cycle obtained from the finite element simulation. The results are taken from the crack center line from different depths. The crack tip is located at a depth of 6 mm in the figure.

to the one recorded with the 10 s cycle at the beginning of the cooling phase, but overall notably weaker in amplitude. The maximum bottom echo is achieved at 1.3 s into the heating phase and it drops around 2 s where it once again rises before the cooling starts. Once the cooling starts, the nonlinear indications increase rapidly, during 1 s, from the free surface towards the crack tip to the depth of 5.5 mm. The indications are visible approximately for the first half of the cooling phase. The bottom echo starts to drop after 0.3 s into the cooling phase. No nonlinear responses were observed beyond 1 s into the cooling phase. Once the heating phase started, no nonlinear response was measured.

In order to further determine the origin of the nonlinear responses, the full array linear response was band pass filtered with $f/2$, $1.5f$ and $2f$ frequencies. The filtered results are shown in Fig. 10 for the 10 s thermal cycle and in Fig. 11 for the 2.5 s cycle. A logarithmic transformation and max-pooling along the sound path was made for better visualisation of the 10 s thermal cycle data (see Fig. 12).

Subharmonic and super harmonic responses follow the nonlinear responses from Fig. 8. No visible signal from the crack tip cold be detected from the heating phase. However, the crack opening can be seen in all harmonic images in Fig. 10, similar to the nonlinear response in Fig. 8. Crack closure is most visible in the $f/2$ subharmonic image, while it is also visible in the super harmonic signal. Unlike in the linear

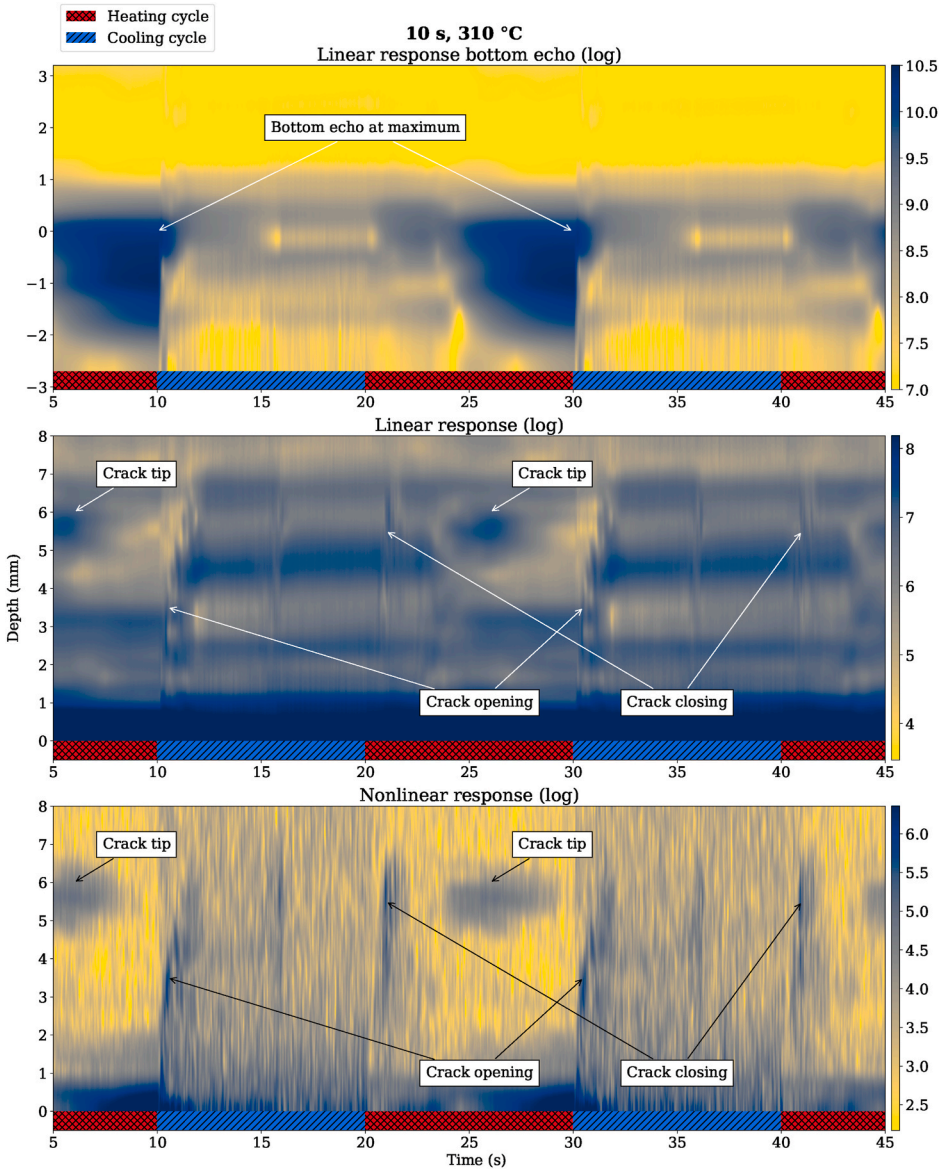

Fig. 8. Linear and nonlinear response for 10 s thermal load cycle. Two cycles are plotted from 5 s from the start of the heating phase to 5 s into the third cycle. The bottom echo of the linear response is shown at the top, the linear response at the middle and the nonlinear response in the bottom. The cooling phase is shown as slash hashed blue line underneath the image and the heating phase as cross hashed red line. (For interpretation of the references to colour in this figure legend, the reader is referred to the Web version of this article.)

and nonlinear response, no response from crack tip can be seen during the heating phase. This indicates that the heating phase signal generates from the central frequency region and is diffracted directly from the tip.

The subharmonic and super harmonic responses in Fig. 11 display the same trends as the nonlinear response in Fig. 9, but the crack tip and opening and closing effects are nearly indistinguishable. Similar to the nonexisting nonlinear response seen in the nonlinear image during the heating phases in Fig. 9, there are no indication of harmonics during the heating phases in Fig. 11.

4. Discussion

The observed nonlinear response is strongly linked to the crack opening displacement and the contact stress on the crack faces. Once the crack is closed and contact stress is high enough, no nonlinear response is produced. This is explained by the fact that the contact stress prevents the crack faces from vibrating and interacting with each other. The 1.5*f* and 2*f* super harmonic responses could be detected mostly during the opening phase when the crack was cooled and also shortly in the beginning of the heating phase with the 10 s thermal cycle loading. Also the subharmonic response was slightly more visible with this load cycle. The presence of these harmonics correlate well with the observed nonlinear responses.

The FAD nonlinear technique was able to detect crack closure until contact stress pressed the crack faces too tightly together. The highest ultrasonic response amplitude occurred with the 10 s thermal cycle at 0.8 s into the heating phase. The FE simulations predicted zero contact pressure at this time and the crack faces were up to 0.6 μm apart, depending on the depth coordinate. In the experiments with the same thermal load case, a nonlinear signal was observed between 0.1 s and 2 s after the cooling phase began when the fully closed crack started to open. However, the crack seemed to open faster than in the FE simulation. We suspect this is due to water flowing into the crack and increasing the cooling rate, whereas in the FE simulation the cooling effect was applied only on the specimen surface. A nonlinear signal was also observed briefly at 6 s into the cooling phase. The simulations predicted that the contact pressure near the crack tip has decreased to below 15 MPa at the corresponding time point. On other locations on the crack face, the FE simulation's opening and closing phases correlate with the nonlinear signal.

Early in the heating phase, the observed nonlinear response does not start at the surface of the specimen as occurs in the cooling phase, but

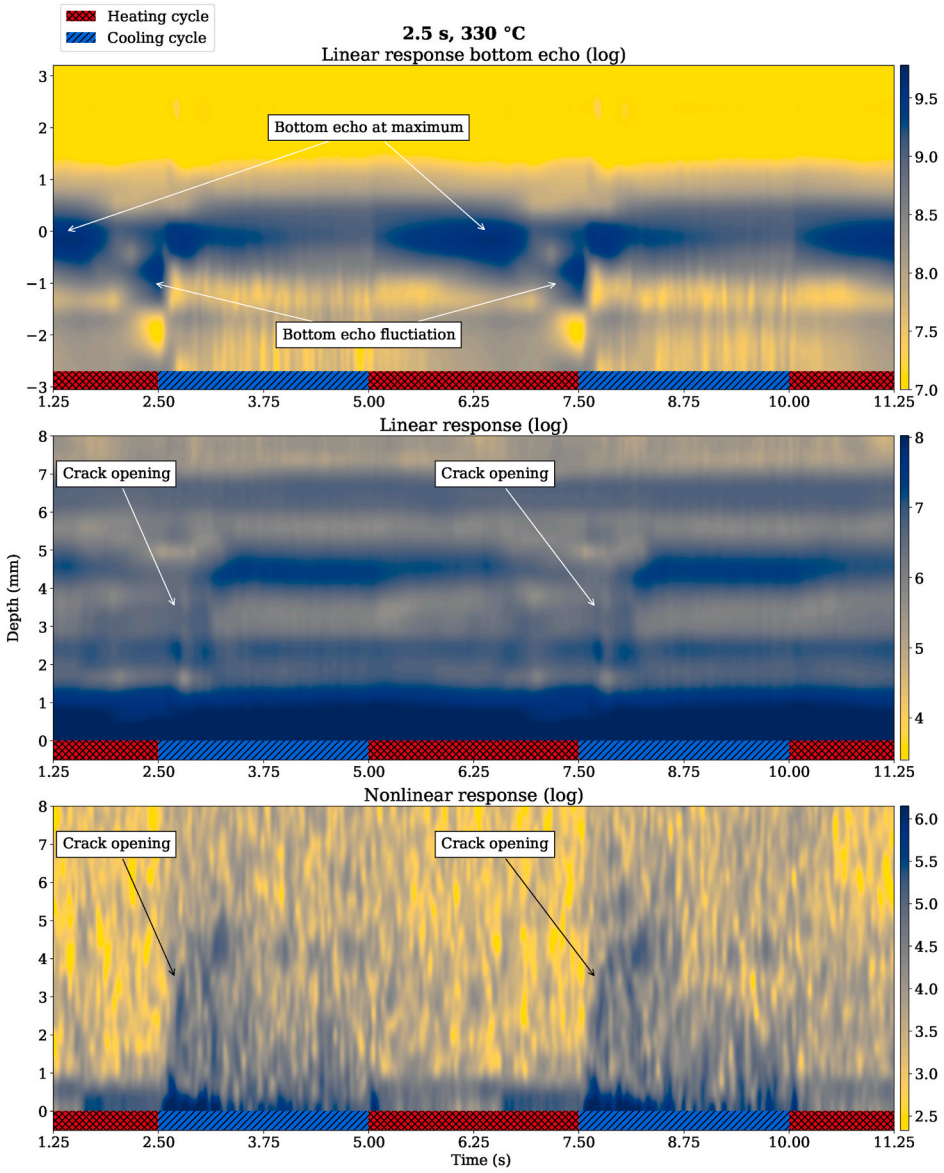

Fig. 9. Linear and nonlinear response for 2.5 s cycle. Two cycles are plotted from 1.25 s from the start of the heating phase to 1.25 s into the third heating phase. The bottom echo of the linear response is shown at the top, linear response at the middle and nonlinear response in the bottom. The cooling phase is shown as slash hashed blue line underneath the image and the heating phase as cross hashed red line. (For interpretation of the references to colour in this figure legend, the reader is referred to the Web version of this article.)

follows well the behavior predicted by the FE simulation. The invisibility of the nonlinear signal at the crack mouth early in the heating phase might be due to water left inside the crack after the cooling phase. The nonlinear signal appears once the crack closure has extended from the sample surface to the middle and tip regions of the crack.

Between 5 s and 9 s within the heating phase of the 10 s thermal cycle, the crack tip can be observed from both linear and nonlinear images. However, this response is not visible in the subharmonics or super harmonics. This indicates that the crack tip has opened enough to diffract the ultrasound directly and no harmonics are produced. Thus, the signal seen in the nonlinear image is mostly linear ultrasound with a higher signal-to-noise ratio than in the simple linear response.

With the shorter thermal cycle, the crack opening behavior was similar during the cooling phase as with the longer thermal cycle. This is due to the same instantaneous water spray cooling method in both cycles. The observed crack opening response is faster than predicted by the FE simulations, where the opening rate was limited by the simulation time step. Similarly, when the heating starts, no nonlinear signal can be observed as the crack closes completely in 0.3 s, which is too fast for the sampling frequency of 26.6 Hz. With the longer thermal cycle, the closure can be seen as it takes approximately 1.6 s. Since the crack is cooled and heated in the shorter cycle for only 2.5 s periods, the thermal inertia prevents the any significant temperature fluctuations from reaching the crack tip depth preventing the crack tip from opening and diffracting the ultrasound like in the longer cycle.

The experiments with two different thermal cycles demonstrate that the nonlinear effect is produced by the rough thermal fatigue crack as there are locations on the crack face, which are close enough to induce the CAN effect. However, as the contact pressure increases, the crack faces become completely pushed together and this *clapping* effect cannot happen. This reduces both the linear response and nonlinear response as the material appears as completely intact. The linear response can be observed when the crack tip is open and diffracts the linear ultrasound. When the crack faces are pushed together, this linear signal can no longer be observed.

While the linear response can size the crack with the same accuracy as the nonlinear response, it is clear that the signal-to-noise ratio of the nonlinear signal is far better than the linear response when the nonlinear signals can be produced. Therefore, the FAD method can be used to detect and size partially closed cracks more accurately than the traditional linear ultrasound. However, the FAD method cannot be utilized if the crack is too open or too closed.

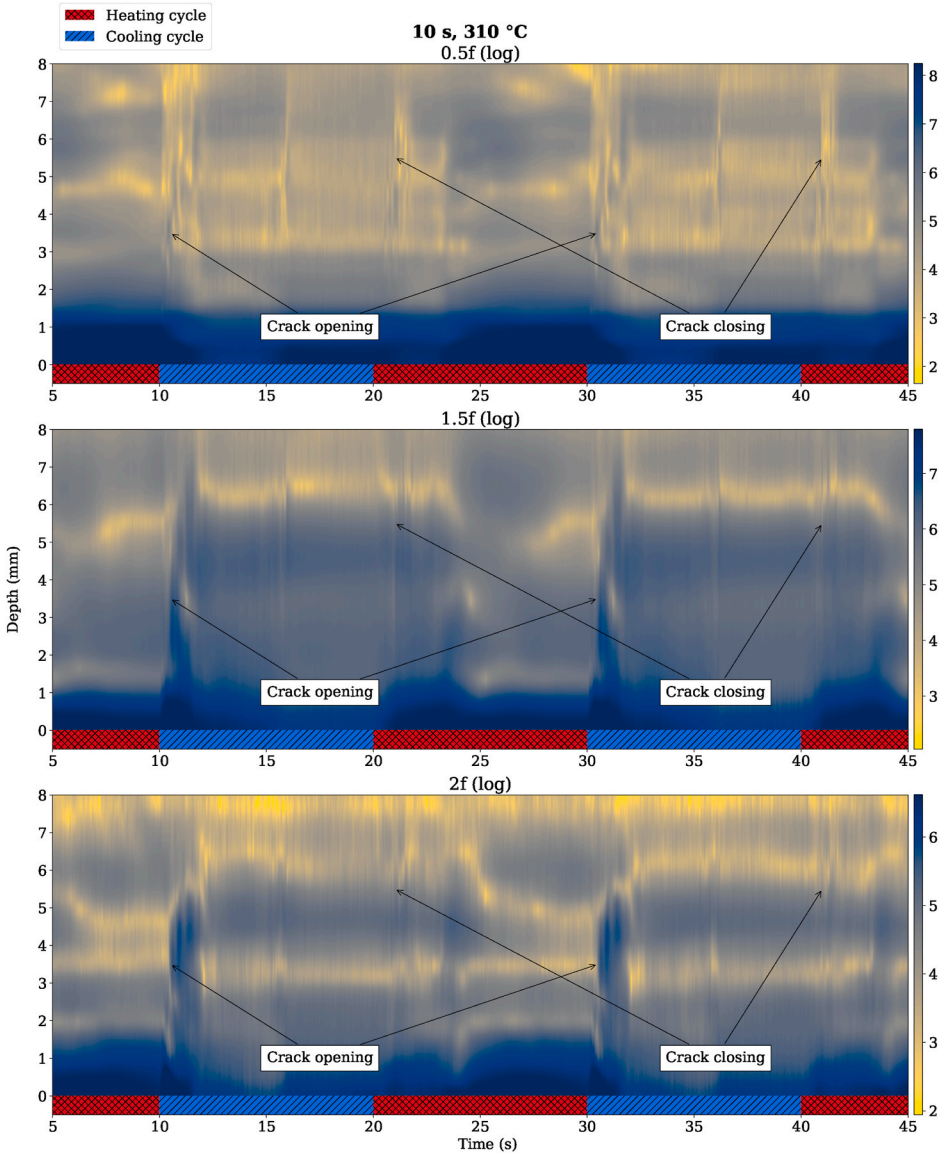

Fig. 10. $f/2$ subharmonic on the top, 1.5f in the middle and 2f in the bottom, determined from the 10 s thermal cycle experiment. Two cycles are plotted from 5 s from the start of the heating phase until 5 s into the third heating phase. The cooling phase is shown as slash hashed blue line underneath the image and the heating phase as cross hashed red line. (For interpretation of the references to colour in this figure legend, the reader is referred to the Web version of this article.)

When the nonlinear response and the FE simulation from the 10 s thermal load cycle are combined in Fig. 12 the nonlinear response are detectable up to 0.6 μm crack opening and up to 450 MPa contact pressure. As stated earlier the water flowing into the crack might cause deviation between the FE simulation and the real experiment, thus transfer from heating to cooling cycle part can be assumed to be closest to the FE simulation. Once the cooling cycle starts, the contact pressure is between 300 and 450 MPa. While the simulation interprets the crack as fully closed at this point, in reality there should be sections which are further apart due to crack roughness.

As the cooling changes into heating cycle in the 10 s thermal loading cycle, nonlinear response is detected once again. However, FE simulation shows the area of the nonlinear response to be open up to 0.6 μm without any contact pressure. As only the upper section of the crack can be seen we suspect that upper sections of the cracks are indeed closer than the simulation would indicate due to roughness of the crack faces. Moreover, the water from the cooling cycle might cause deviation to the FE simulation.

5. Conclusion

The FAD approach is an effective way to produce a nonlinear response with conventional phased array equipment. The nonlinear response can make it possible to characterize and size a crack that is partially closed or the crack tip is closed. However, if the contact pressure is too high, the crack faces are completely pushed together and the *clapping* of the crack faces is prevented and the crack does not generate any ultrasonic response. The nonlinear effect is also diminished if the crack faces are too far apart. In the current experiments, the best signal-to-noise ratio with the FAD method was achieved when the crack opening displacement was approximately less than 0.6 μm and the contact pressure of the crack faces was approximately less than 450 MPa, as predicted by the FE simulations. However, as there was water inflow into the crack during the experiments, the limits quantified by the FE simulations without explicit consideration of the cooling water are assessed to be too strict. That is, the nonlinear response from a completely dry crack is expected to be obtained with larger crack opening displacements and higher contact pressures than in the current

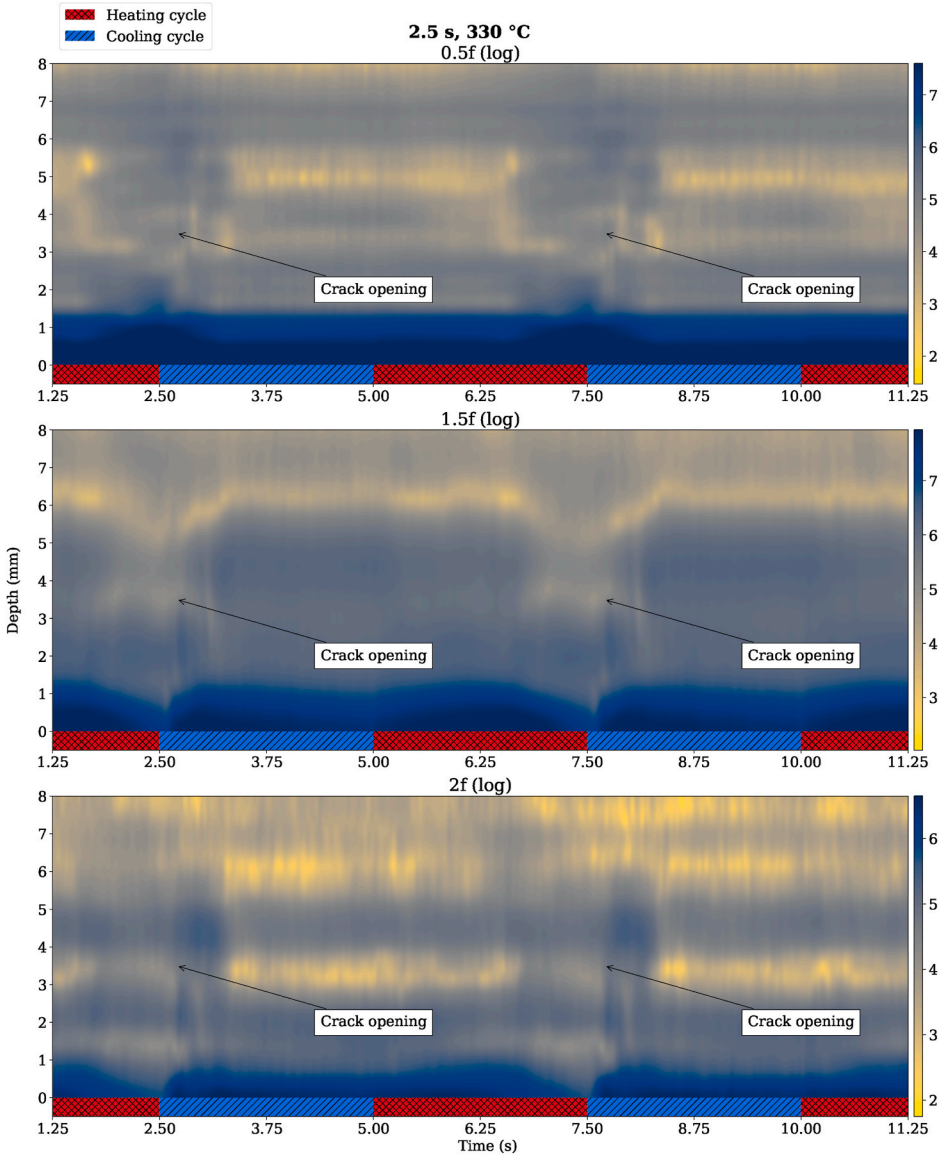

Fig. 11. $f/2$ subharmonic response on the top, 1.5f in the middle and 2f in the bottom, determined from the 2.5 thermal cycle experiment. Two cycles are plotted from 1.25 s from the start of the heating phase until 1.25 s into the third heating phase. The cooling phase is shown as slash hashed blue line underneath the image and the heating cycle as cross hashed red line. (For interpretation of the references to colour in this figure legend, the reader is referred to the Web version of this article.)

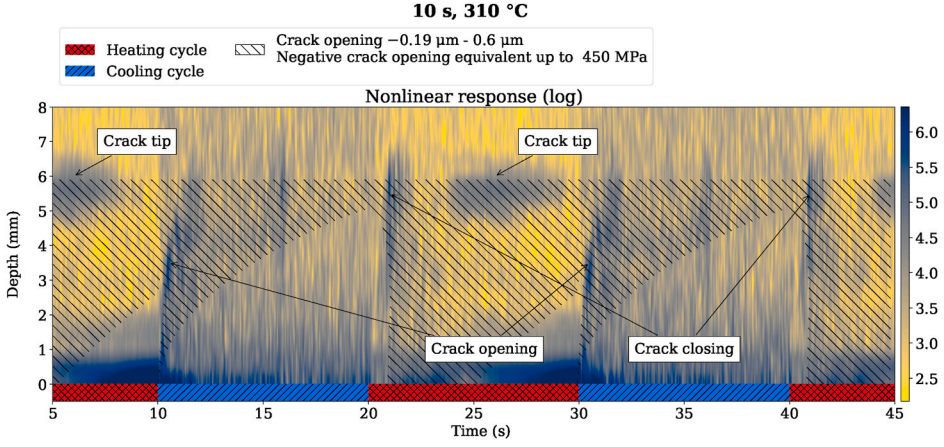

Fig. 12. Combined nonlinear response and FE simulation for the 10 s thermal load cycle. The cooling cycle is shown as slash hashed blue line underneath the image and the heating cycle as cross hashed red line. The estimated crack opening between −0.19 – 0.6 µm is the transparent back slashed area. Negative crack opening represents contact pressure up to 450 MPa. (For interpretation of the references to colour in this figure legend, the reader is referred to the Web version of this article.)

experiments.

Declaration of competing interest

The authors declare that they have no known competing financial interests or personal relationships that could have appeared to influence the work reported in this paper.

Acknowledgements

This paper was funded by the Finnish radiation safety program SAFIR2022. Trueflaw contributed the thermal fatigue cycle for the flaw. All contributions are greatfully acknowledged.

References

[1] Krautkrämer J, Krautkrämer H. Ultrasonic testing of materials. Springer-Verlag; 1983. URL: https://books.google.fi/books?id=AvwrAAAAIAAJ.
[2] Birks A, Green R, McIntire P. Nondestructive testing handbook. In: Ultrasonic testing. 3 ed., vol. 7. Columbus: American Society for Nondestructive Testing; 2007.
[3] Schmerr LW. Fundamentals of ultrasonic nondestructive evaluation. 2 ed. Springer International Publishing; 2016.
[4] Wolf E. Fatigue crack closure under cyclic tension. Eng Fract Mech 1970;2:37–45. URL: https://www.sciencedirect.com/science/article/pii/0013794470900287. doi:10.1016/0013-7944(70)90028-7.
[5] Steuwer A, Rahman M, Shterenlikht A, Fitzpatrick M, Edwards L, Withers P. The evolution of crack-tip stresses during a fatigue overload event. Acta Mater 2010;58:4039–52. URL: https://www.sciencedirect.com/science/article/pii/S1359645410001588. doi:10.1016/j.actamat.2010.03.013.
[6] Takumi T, Katsuhiko F, Koji A. Microstructural characterization of scc crack tip and oxide film for sus 316 stainless steel in simulated pwr primary water at 320 c. J Nucl Sci Technol 2005;42:225–32. https://doi.org/10.1080/18811248.2005.9726383. doi:10. 1080/18811248.2005.9726383, arXiv:10.1080/18811248.2005.9726383.
[7] Ohara Y, Yamamoto S, Mihara T, Yamanaka K. Ultrasonic evaluation of closed cracks using subharmonic phased array. Jpn J Appl Phys 2008;47:3908–15. https://doi.org/10.1143/jjap.47.3908. URL:.
[8] Solodov I, Krohn N, Busse G. Can: an example of nonclassical acoustic nonlinearity in solids. Ultrasonics 2002;40:621–5. URL: http://www.sciencedirect.com/science/article/pii/S0041624X02001865. doi:10.1016/S0041-624X(02)00186-5.
[9] Bouakaz A, Jong N. Native tissue imaging at superharmonic frequencies. Ultrasonics, Ferroelectrics and Frequency Control. IEEE Transactions on 2003;50:496–506. https://doi.org/10.1109/TUFFC.2003.1201462.
[10] Yamanaka K, Mihara T, Tsuji T. Evaluation of closed cracks by model analysis of subharmonic ultrasound. Jpn J Appl Phys 2004;43:3082–7. https://doi.org/10.1143/jjap.43.3082. URL:.
[11] Ohara Y, Mihara T, Sasaki R, Ogata T, Yamamoto S, Kishimoto Y, Yamanaka K. Imaging of closed cracks using nonlinear response of elastic waves at subharmonic frequency. Appl Phys Lett 2007;90:011902. https://doi.org/10.1063/1.2426891. doi:10.1063/1. 2426891, arXiv:10.1063/1.2426891.
[12] Solodov I, Asainov A, Sel Len K. Non-linear saw reflection: experimental evidence and nde applications. Ultrasonics 1993;31:91–6. URL: http://www.sciencedirect.com/science/article/pii/0041624X93900382. doi:10.1016/0041-624X(93)90038-2.
[13] Solodov IY. Ultrasonics of non-linear contacts: propagation, reflection and nde-applications. Ultrasonics 1998;36:383–90. URL: http://www.sciencedirect.com/science/article/pii/S0041624X97000413. doi:10.1016/S0041-624X(97)00041-3. ultrasonics International 1997.
[14] Biwa S, Nakajima S, Ohno N. On the acoustic nonlinearity of solid-solid contact with pressure-dependent interface stiffness. J Appl Mech 2004;71:508–15. https://doi.org/10.1115/1.1767169. arXiv: https://asmedigitalcollection.asme.org/appliedmechanics/article-pdf/71/4/508/5471355/508_1.pdf.
[15] Haupert S, Renaud G, Schumm A. Ultrasonic imaging of nonlinear scatterers buried in a medium. NDT E Int 2017;87:1–6. URL: http://www.sciencedirect.com/science/article/pii/S0963869516303206. doi:10.1016/j.ndteint.2016.12.010.
[16] Haupert S, Ohara Y, Carcreff E, Renaud G. Fundamental wave amplitude difference imaging for detection and characterization of embedded cracks. Ultrasonics 2019;96:132–9. URL: http://www.sciencedirect.com/science/article/pii/S0041624X18304177. doi:10.1016/j.ultras.2019.02.003.
[17] Ikeuchi M, Jinno K, Ohara Y, Yamanaka K. Improvement of closed crack selectivity in nonlinear ultrasonic imaging using fundamental wave amplitude difference. Jpn J Appl Phys 2013;52. https://doi.org/10.7567/JJAP.52.07HC08.
[18] Ohara Y, Nakajima H, Haupert S, Tsuji T, Mihara T. Nonlinear ultrasonic phased array with fixed-voltage fundamental wave amplitude difference for high-selectivity imaging of closed cracks. J Acoust Soc Am 2019;146:266–77. https://doi.org/10.1121/1.5116017. doi:10.1121/1.5116017.
[19] Kemppainen M, Virkkunen I, Pitkänen J, Paussu R, Hänninen H. Advanced flaw production method for in-service inspection qualification mock-ups. Nucl Eng Des 2003;224:105–17.
[20] Virtanen, P., Gommers, R., Oliphant, T.E., Haberland, M., Reddy, T., Cournapeau, D., Burovski, E., Peterson, P., Weckesser, W., Bright, J., van der Walt, S.J., Brett, M., Wilson, J., Millman, K.J., Mayorov, N., Nelson, A.R.J., Jones, E., Kern, R., Larson, E., Carey, C.J., Polat, İ., Feng, Y., Moore, E.W., VanderPlas, J., Laxalde, D., Perktold, J., Cimrman, R., Henriksen, I., Quintero, E.A., Harris, C.R., Archibald, A. M., Ribeiro, A.H., Pedregosa, F., van Mulbregt, P., SciPy 1.0 contributors, 2020. SciPy 1.0: fundamental algorithms for scientific computing in Python. Nat Methods 17, 261–272. doi:10.1038/s41592-019-0686-2..
[21] USA, D.S.S.C.P.R.. Abaqus software. 2019.
[22] Asme. Asme boiler and pressure vessel code, section ii. Part D, Properties. 2017 (Metric).
[23] Scalerandi M, Gliozzi AS, Bruno CLE, Masera D, Bocca P. A scaling method to enhance detection of a nonlinear elastic response. Applied Physics Letters 2008;92. https://doi.org/10.1063/1.2890031.